Physics characterization and frequency stability of the pulsed rubidium maser

Aldo Godone, Salvatore Micalizio, Filippo Levi, and Claudio Calosso
Istituto Nazionale di Ricerca Metrologica, INRIM, Strada delle Cacce 91, 10135 Torino, Italy
(Received 2 May 2006; published 2 October 2006)

In this paper we report the theoretical and experimental characterization of a pulsed optically pumped vapor-cell frequency standard based on the detection of the free-induction decay microwave signal. The features that make this standard similar to a pulsed passive maser are presented. In order to predict and optimize the frequency stability, thermal and shot noise sources are analyzed, as well as the conversions of the laser and microwave fluctuations into the output frequency. The experimental results obtained with a clock prototype based on ^{87}Rb in buffer gas are compared with the theoretical predictions, showing the practical possibility to implement a frequency standard limited in the medium term only by thermal drift. The achieved frequency stability is $\sigma_y(\tau)=1.2\times10^{-12}\tau^{-1/2}$ for measurement times up to $\tau\approx10^5$ s. It represents one of the best results reported in literature for gas cell frequency standards and is compliant with the present day requirements for on board space applications.

DOI: 10.1103/PhysRevA.74.043401 PACS number(s): 32.80.Bx, 32.70.Jz, 06.30.Ft

I. INTRODUCTION

The recent efforts to improve the performances of the vapor-cell frequency standards, aiming to reach a short-term relative frequency stability of $1\times10^{-12}\tau^{-1/2}$ up to measuring times $\tau=10\,000$ s, are solicited, among others, by the field of satellite radio-navigation. In this framework, several approaches have been considered and are under development to match the above specifications: the rf-optical double-resonance technique [1], the standards based on the electromagnetically induced transparency (EIT) effect [2], the coherent population trapping (CPT) maser [3], and the pulsed optically pumped (POP) frequency standard [4]. We shall report in this paper a theoretical treatment of the POP operation and the experimental results obtained with a laboratory prototype based on the ^{87}Rb atom which reaches the goal of an Allan standard deviation [5] $\sigma_y(\tau)=1\times10^{-12}\tau^{-1/2}$ for $1\leqslant\tau\leqslant10^5$ s.

The original idea conceived in the early 1960s by Alley [6] has been developed in our system that makes use of: (i) a diode laser for the optical pumping, (ii) the Ramsey technique to interrogate the atoms, and (iii) the free-induction decay signal for the detection of the clock transition. These three operation phases are controlled through gated electronics, as shown in the schematic setup of Fig. 1.

The Ramsey interaction provides a clock signal line shape independent from the laser and from the rf power and in addition allows a strong reduction of the cavity-pulling effect via a proper choice of the microwave pulse area, as discussed in Ref. [7]. The detection of the microwave decay mostly avoids the transfer of the laser amplitude fluctuations to the clock signal. The pulsed operation, whose timing pattern is shown in Fig. 2, separates in time the pumping, the interrogation, and the detection phases and cancels in principle the light-shift effect [8,9] that highly impairs the stability of the rf-optical frequency standards. The detrimental effect of the pulsed operation on the short-term stability is then avoided with gated electronics.

In our experiment we have chosen the ^{87}Rb atom for its lower nuclear spin ($I=3/2$) that reduces the spread of the atomic population among the Zeeman sublevels and for the larger volume of the active medium that can be used if compared to ^{133}Cs. The low pressure ^{87}Rb vapor is contained in a quartz cell of length L with buffer gas to increase the interaction time between the atoms and the microwave field through the Dicke effect. The microwave cavity shown in Fig. 1 is tuned to the ^{87}Rb hyperfine transition frequency and operates on the TE_{011} electromagnetic mode. The laser light is tuned to the optical D_1 transition ($\lambda\approx795$ nm) and its free space TEM_{00} mode is coupled to the cell via a telescope in order to reach a beam waist of radius ρ_w ($1/e$ of the laser intensity) equal to the desired transverse radius of the active medium. Further details will be reported in the following sections. In particular, in Sec. II we will report a theoretical treatment of the POP frequency standard showing also that, though pulsed, it may be considered to belong to the class of the passive masers. In Sec. III the frequency stability will be analyzed in order to define the operating conditions necessary to reach the goal fixed at the beginning of this section. In Secs. IV and V the experimental setup and the obtained results will be, respectively, described and reported. Finally, a comparison of our data with those reported in literature will be presented in Sec. VI, as well as the perspectives for future improvements.

II. THEORY

In this section we introduce the main theoretical aspects of the POP operation with some extensions with respect to the theory already reported in Ref. [7].

The optical pumping is performed through a semiconductor laser whose beam is linearly polarized with the wave vector parallel to the quantization axis $\hat{\mathbf{z}}$, defined by a static magnetic field $\mathbf{B}_0=B_0\hat{\mathbf{z}}$. The σ^+ and σ^- light components couple all the $|^2S_{1/2};F=2\rangle-|^2P_{1/2};F=1\rangle$ transitions, as indicated in Fig. 3, producing the required population difference between the clock levels $|\mu'\rangle=|^2S_{1/2};F=2,m_F=0\rangle$ and $|\mu\rangle=|^2S_{1/2};F=1,m_F=0\rangle$. In the figure, γ_1 and γ_2 are, respectively, the population difference and the hyperfine coherence relaxation rates in the ground state and Γ^* the decay rate of

 ©2006 The American Physical Society

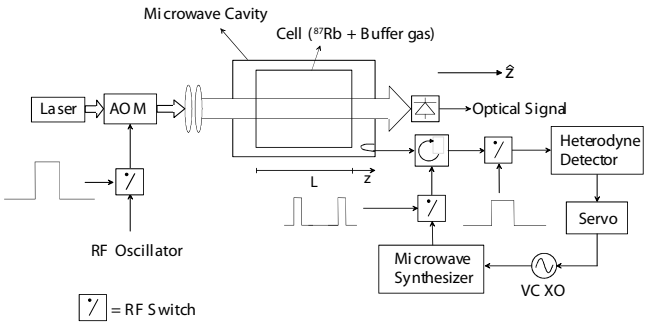

FIG. 1. Schematic setup of the POP frequency standard. AOM: acousto-optic modulator. VCXO: voltage controlled crystal oscillator.

the excited state $|m\rangle=|^2P_{1/2};F=1\rangle$; the interaction with the buffer gas is included in the definition of the decay rates.

In the case of an optically thin medium, we have calculated the density matrix ($\hat{\rho}$) elements solving the Liouville equation for the 11 levels of Fig. 3 in order to evaluate the population inversion $\Delta=\rho_{\mu'\mu'}-\rho_{\mu\mu}$ achieved after a laser pulse of duration t_p.

The result is shown in Fig. 4 where $-\Delta$ is reported vs t_p for different pumping rates $\Gamma_p=\omega_R^2/2\Gamma^*$, ω_R being the Rabi frequency associated to the optical transition. The curves reported in the figure have been obtained for $\gamma_1\approx\gamma_2=300\ \mathrm{s}^{-1}$ and $\Gamma^*=3\times10^9\ \mathrm{s}^{-1}$ that reproduce a typical experimental condition (see Sec. IV), and assuming for the relaxation rates among the Zeeman sublevels in $^2S_{1/2}$ and in $^2P_{1/2}$ the values $\gamma_Z(2S_{1/2})=20\,000\ \mathrm{s}^{-1}$ [10] and $\gamma_Z(2P_{1/2})=3\times10^9\ \mathrm{s}^{-1}$, respectively. The results of Fig. 4 include the effect of the coherent population trapping in the states $|^2S_{1/2};F=2\rangle$ due to Λ and V couplings. Without loss of generality, we will consider in the following the simpler three-level system shown in Fig. 5 to describe the POP atomic clock. We will assume an effective atomic density $n_e\leqslant n/4$ to take into account the above computations (n being the real atomic density) and keep $\mathrm{Tr}(\hat{\rho})=1$ also in the simplified scheme.

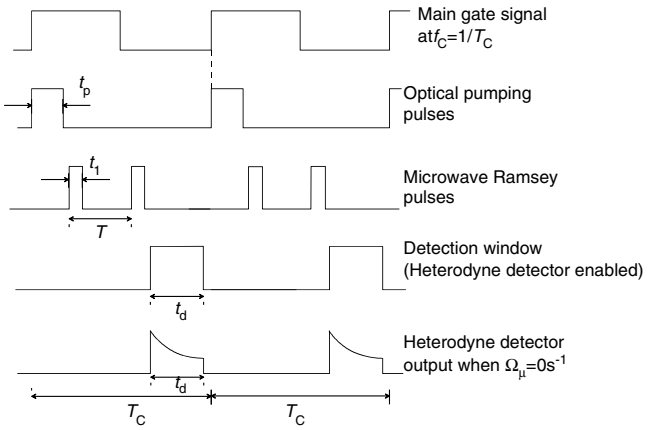

FIG. 2. Timing pattern T_C cycle time, t_p optical pumping time, t_1 Rabi time, T Ramsey time, and Ω_μ detuning of the microwave frequency ω_0 with respect to the hyperfine frequency $\omega_{\mu\mu'}$ ($\Omega_\mu=\omega_0-\omega_{\mu\mu'}$).

In the formalism of the ensemble-averaged density matrix formalism and in the rotating wave approximation, the following set of equations holds [7,11]:

$$\dot{\Delta}+(\gamma_1+\Gamma_p)\Delta=-2b_e\,\mathrm{Im}(e^{-i\phi_e}\delta_{\mu\mu'})-2\,\mathrm{Im}(\tilde{b}_i^*\delta_{\mu\mu'})-\Gamma_p,$$

$$\dot{\delta}_{\mu\mu'}+\left[\gamma_2+\Gamma_p+i\left(\Omega_\mu-\Gamma_p\delta_0-\frac{\omega_R^2}{4\omega_{\mu\mu'}}\right)\right]\delta_{\mu\mu'}=i\frac{b_e}{2}e^{i\phi_e}\Delta+i\frac{\tilde{b}_i}{2}\Delta,$$

$$\dot{\rho}_{mm}+\Gamma^*\rho_{mm}=\Gamma_p(1+\Delta),$$

$$\frac{\partial\omega_R}{\partial z}+\frac{1}{c}\frac{\partial\omega_R}{\partial t}=-\alpha\frac{\omega_R}{2\Gamma^*}(1+\Delta),$$

$$\tilde{b}_i(t)=2i\bar{k}e^{i\psi}H_{az}(\rho,z)\int_{V_a}\delta_{\mu\mu'}(\rho,z,t)H_{az}(\rho,z)dV$$

$$(dV=2\pi\rho d\rho dz). \tag{1}$$

The first three differential equations of the system (1) come from the Liouville equation. In particular, the first describes the time evolution of the population difference between the ground state hyperfine levels, where in the right-hand side the following pumping rates are made explicit: (i) the external Rabi frequency $\tilde{b}_e$ related to the applied microwave field, (ii) the internal Rabi frequency $\tilde{b}_i$ due to the microwave field sustained by the cavity mode and excited by the atomic magnetization, and (iii) the laser field.

The second and third equations of system (1) refer to the time evolution of the hyperfine coherence $\rho_{\mu\mu'}=\delta_{\mu\mu'}e^{i\omega_0 t}$, $\delta_{\mu\mu'}$ being the slowly varying part, and of the excited state population ρ_{mm}. They have been derived under the hypotheses $\omega_R\ll\Gamma^*$, $\Omega_\mu\ll\Gamma^*$, $|b_e|\ll\Gamma^*$, and $\delta_0=2\Delta_0/\Gamma^*\ll1$ that are widely satisfied in the experimental operating conditions of interest; system (1) also includes in a self-consistent way the feedback action of the microwave cavity on the atomic ensemble through the terms proportional to $\tilde{b}_i$. In the second equation, the terms $\Gamma_p\delta_0$ and $\omega_R^2/4\omega_{\mu\mu'}$ represent the resonant and the off-resonant light-shift contributions [12].

The fourth equation of system (1) is deduced from the Maxwell equations (in the slowly varying amplitude approximation) and accounts for the laser absorption along the cell of optical length $\zeta=\alpha L/\Gamma^*$, α being the linear absorption coefficient.

Finally, the fifth equation of system (1), also known as the Slater equation [5], yields the Rabi frequency related to the microwave field induced by the atomic system magnetization. In this last equation

$$\bar{k}=\frac{\mu_0\mu_B^2Q_Ln_e}{\hbar}, \tag{2}$$

where $\hbar$ is the reduced Planck constant, μ_0 the vacuum permeability, μ_B the Bohr magneton, and Q_L the loaded cavity quality factor. Moreover, ψ is the reduced cavity detuning:

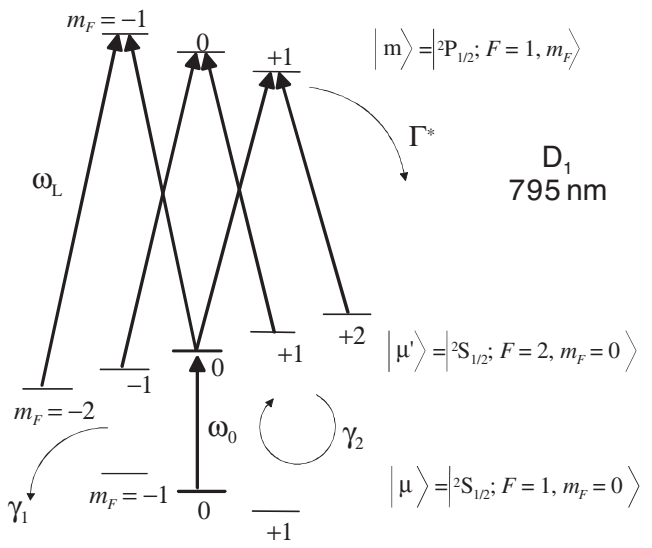

FIG. 3. Atomic levels of ^{87}Rb involved in the optical pumping; ω_L and ω_0 are the angular laser and microwave frequencies.

$$\psi = 2Q_L \frac{\Delta\omega_c}{\omega_{\mu\mu'}}, \tag{3}$$

$\Delta\omega_c = \omega_c - \omega_0$ being the cavity detuning and $\omega_{\mu\mu'}$ the unperturbed hyperfine frequency; we will assume $\psi \ll 1$. H_{az} is the longitudinal magnetic component of the TE_{011} eigenvector in cylindrical coordinates (ρ, φ, and z):

$$H_{az}(\rho,z) = H_0 J_0\left(\frac{x'_{01}}{a}\rho\right)\cos\left(\frac{\pi}{d}z\right), \tag{4}$$

where x'_{01} is the first root of the derivative of the Bessel function $J_0(x)$, a and d the radius and the length of the cavity, and H_0 a normalization constant. The Rabi frequency $\tilde{b}_e$ has obviously the same dependence on ρ and z as H_{az}. It is convenient to assume for H_0 the value

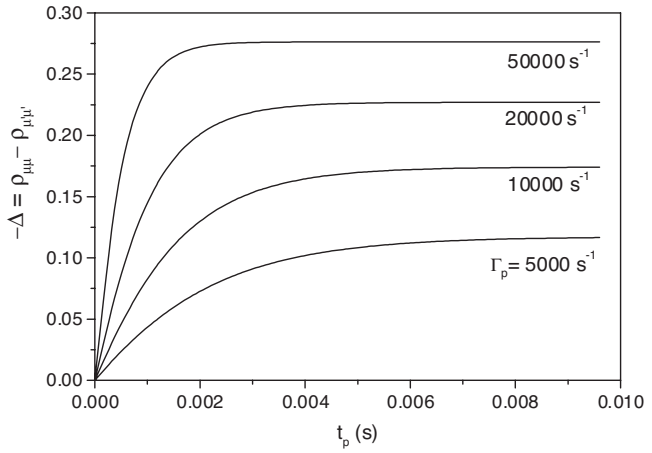

FIG. 4. Calculated population inversion vs the pulse duration, for different pumping rates.

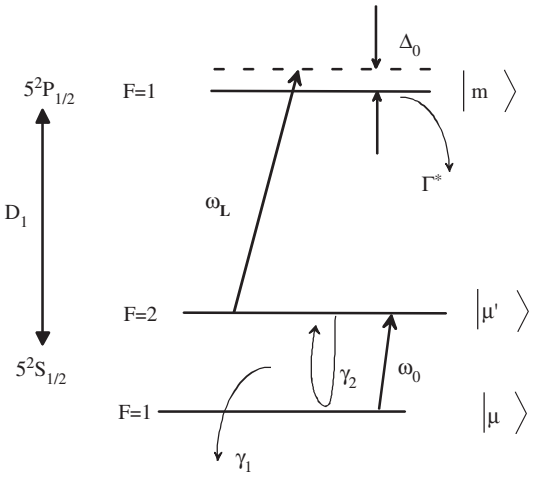

FIG. 5. Equivalent three-level system considered in the text; Δ_0 is the laser detuning with respect to the optical transition $\Delta_0 = \omega_L - \omega_{\mu' m}$.

$$H_0 = \sqrt{\frac{\eta'}{V_a}}, \tag{5}$$

where η' is the cavity filling factor [5] and V_a the volume of the active medium defined by the cell length and by the laser beam cross section. With this normalization, all the expressions reduce to those reported in literature when the assumption $H_{az} \approx$ const is made. In the most general case, the solutions obtained from Eqs. (1) for Δ, $\delta_{\mu\mu'}$, ρ_{33}, ω_R, and $\tilde{b}_i$ depend on the spatial coordinates ρ and z. As already recalled in Sec. I, we observe the clock transition via the free-induction decay signal after microwave interaction; the power dissipated in the cavity is

$$P_a(t) = \frac{1}{2}\hbar\omega_{\mu\mu'}N_a\frac{\bar{k}}{V_a}\left|\int_{V_a} 2\delta_{\mu\mu'}(\rho,z,t)H_{az}(\rho,z)dV\right|^2, \tag{6}$$

where $N_a = n_e V_a$ is the number of atoms effectively involved in the interaction and $t=0$ the end of the second Ramsey pulse.

The solution of the partial derivatives integrodifferential equations of system (1) may be found only numerically. In order to achieve a better insight of the physical behavior of the POP atomic clock with closed-form solutions, it is convenient to examine the system under the hypothesis $H_{az} \approx$ const and $\omega_R \approx$ const for each ρ and z. This means considering a small cell in the center of the cavity and an optically thin medium. We shall introduce the spatial inhomogeneities only when necessary to explain some departures of the experimental data from the theoretical predictions. In the above hypothesis, Eq. (6) becomes

$$P_a(t) = \frac{1}{2}\hbar\omega_{\mu\mu'}N_a k|2\delta_{\mu\mu'}|^2, \tag{7}$$

where $k = \eta'\bar{k}$. The fourth and the fifth equations of system (1) turn out simplified as follows:

$$\omega_R = \text{const}, \tag{8}$$

$$\bar{b}_i = 2ike^{i\psi}\delta_{\mu\mu'}, \tag{9}$$

while the third one remains uncoupled and the atomic system is described by the following set of equations:

$$\dot{\Delta} + (\gamma_1 + \Gamma_p)\Delta = 2b_e \,\text{Re}\,\delta_{\mu\mu'} + 4k|\delta_{\mu\mu'}|^2 - \Gamma_p,$$

$$\dot{\delta}_{\mu\mu'} + \left[\gamma_2 + \Gamma_p + i\left(\Omega_\mu - \Gamma_p\delta_0 - \frac{\omega_R^2}{4\omega_{\mu\mu'}}\right)\right]\delta_{\mu\mu'} = -\frac{b_e}{2}\Delta - k\Delta(1+i\psi)\delta_{\mu\mu'}. \tag{10}$$

The phase of $\tilde{b}_e$ is arbitrary and we have chosen in Eqs. (10) $\tilde{b}_e = b_e e^{i\pi/2}$ with b_e real.

We now report the solutions of Eqs. (10) for the different phases of the timing sequence (Fig. 2).

In the optical pumping interval $b_e = 0\ \text{s}^{-1}$ and $k = 0\ \text{s}^{-1}$, since the cavity feedback effect is completely negligible; the solution of Eqs. (10) is easily found to be at $t = t_p$:

$$\Delta(t_p) = \Delta(0)e^{-(\gamma_1+\Gamma_p)t_p} - \frac{\Gamma_p}{\gamma_1+\Gamma_p}[1 - e^{-(\gamma_1+\Gamma_p)t_p}],$$

$$\delta_{\mu\mu'}(t_p) = \delta_{\mu\mu'}(0)e^{-(\gamma_2+\Gamma_p)t_p}e^{-i(\Omega_\mu - \Gamma_p\delta_0 - \omega_R^2/4\omega_{\mu\mu'})t_p}, \tag{11}$$

where $\Delta(0)$ and $\delta_{\mu\mu'}(0)$ are the initial values at the beginning of the laser pulse. The first relation gives the population inversion reached before the microwave interaction while the second one yields the residual microwave coherence at the end of the laser pulse. In order to avoid the light-shift effect contained in the rotating term, it is necessary to satisfy the condition $\Gamma_p t_p \gg 1$. In the case of an optically thick medium, this condition becomes [7]

$$(\Gamma_p - \zeta\gamma_1)t_p \gg 1. \tag{12}$$

When Eq. (12) is satisfied we have from Eqs. (11):

$$\Delta(t_p) = -\frac{\Gamma_p}{\gamma_1+\Gamma_p} \equiv \Delta_i,$$

$$\delta_{\mu\mu'}(t_p) = 0 + i0, \tag{13}$$

that, in turn, play the role of initial conditions for the microwave interaction region. During the first microwave pulse $\Gamma_p = 0$, $t_1 \ll \gamma_1^{-1}, \gamma_2^{-1}$, moreover, also in this case $k = 0$ since the cavity feedback on the atoms is negligible ($b_e \gg |\tilde{b}_i|$); an analytical solution of Eqs. (10) then exists [5,7]. Since we are looking for the central Ramsey fringe only, we can use the usual approximation $\Omega_\mu = 0$, disregarding then the Rabi pedestal:

$$\Delta(t_1) = \Delta(t_p)\cos\theta + 2\,\text{Re}\,\delta_{\mu\mu'}(t_p)\sin\theta,$$

$$\text{Re}\,\delta_{\mu\mu'}(t_1) = \text{Re}\,\delta_{\mu\mu'}(t_p)\cos\theta - \frac{\Delta(t_p)}{2}\sin\theta,$$

$$\text{Im}\,\delta_{\mu\mu'}(t_1) = \text{Im}\,\delta_{\mu\mu'}(t_p). \tag{14}$$

In Eqs. (14) $\theta = b_e t_1$ is the microwave pulse area.

In the free decay interval $b_e = 0$ and the system (10) can be written as

$$\dot{\Delta} + \gamma_1\Delta = 4k|\delta_{\mu\mu'}|^2,$$

$$\dot{\delta}_{\mu\mu'} + (\gamma_2 + i\Omega_\mu)\delta_{\mu\mu'} = -k\Delta(1+i\psi)\delta_{\mu\mu'}. \tag{15}$$

An analytical solution of Eqs. (15) may be found when $\gamma_1 = \gamma_2 \equiv \gamma$ and the initial conditions (13) for the microwave pulse hold [5,7,13]; using for Eqs. (15) the initial values provided by Eqs. (14) and expressing the coherence term as $\delta_{\mu\mu'} = Me^{i\phi}$ we have

$$\Delta(t) = -|\Delta_i|e^{-\gamma t}\tanh[A(t) - \text{sgn}(\Delta_i)\tanh^{-1}\cos\theta],$$

$$M(t) = \frac{|\Delta_i|}{2}e^{-\gamma t}\,\text{sech}[A(t) - \text{sgn}(\Delta_i)\tanh^{-1}\cos\theta],$$

$$\phi(t) = \phi(0) - \Omega_\mu t - \phi_0(t), \tag{16}$$

where $\phi(0) = 0$ or π if $\sin\theta > 0$ or $\sin\theta < 0$, and

$$A(t) = \frac{k}{\gamma}|\Delta_i|(1 - e^{-\gamma t}), \tag{17}$$

$$\phi_0(t) = \psi\ln\{\cosh A(t) - \text{sgn}(\Delta_i)\cos\theta\sinh A(t)\}. \tag{18}$$

In Eqs. (16)–(18) $t = 0$ is the origin of the free-induction decay time T. The term $\phi_0(t)$ is due to the dephasing of the microwave coherence induced by the cavity feedback and gives the cavity-pulling shift $\Delta\omega_{cp}$ at the end of the Ramsey time:

$$\Delta\omega_{cp} = -\frac{\phi_0(t)}{T}. \tag{19}$$

The second Ramsey pulse is described by relations similar to Eqs. (14), but with the initial values provided by Eqs. (16) with $t = T$. In the detection region the free decay of the coherence may be simply described by the term $e^{-\gamma t}$ because the feedback action of the cavity is typically negligible due to the previous decay during the Ramsey time. Following all the steps reported so far the power dissipated by the atoms in the cavity may be evaluated through Eq. (7). In the case of particular interest for the experiments [7], $\theta = \pi/2$ and $\psi = 0$, we obtain:

$$P_a(t) = \frac{1}{2}\hbar\omega_{\mu\mu'}N_a k|\Delta_i|^2 e^{-2\gamma T} \times\{\tanh^2 A(T) + \sin^2\Omega_\mu T\,\text{sech}^2 A(T)\}e^{-2\gamma t}, \tag{20}$$

where now $t = 0$ is the beginning of the detection interval t_d. The power $P_d(t)$ coupled to the heterodyne detector is

$$P_d(t) = \frac{\beta}{\beta+1}P_a, \tag{21}$$

β being the cavity coupling factor.

The full width at half maximum (FWHM) $\Delta\nu_{1/2}$ of the central Ramsey fringe is easily deduced from Eq. (20) and turns out $\Delta\nu_{1/2}=1/4T$, so that the atomic quality factor is $Q_a=4T\nu_{\mu\mu'}$ (see also Ref. [7]). It is interesting to observe that Eq. (20) predicts an increased "background" emission and a decreased Ramsey oscillation amplitude when the cavity feedback increases. From the theoretical point of view it is interesting to consider the two limits of Eq. (20):

(a) $\lim_{k\to 0} P_a(t)=0$ for each γ and t;

(b) $\lim_{\gamma\to 0} P_a(t)=\frac{1}{2}\hbar\omega_{\mu\mu'}N_a k|\Delta_i|^2\{\tanh^2(k|\Delta_i|T)+\mathrm{sech}^2(k|\Delta_i|T)\sin^2\Omega_\mu T\}$.

The limit (a) makes evident that no power is delivered by the atoms after the second Ramsey pulse ($t=0$) without the interaction with the microwave cavity ($k=0$ if $Q_L=0$). The limit (b) makes clear that the free-induction decay takes place, as expected, also without the atom buffer-gas interaction ($\gamma\to 0$). The above observations lead one to consider the power emitted by the atomic ensemble as a stimulated emission typical of maser devices. Moreover, when $k/\gamma<4$ the atomic system is certainly below threshold [14] so that we may ascribe it to the class of passive masers.

Finally, we report the number N of the microwave photons that are detected during the interval t_d via a coherent square-wave modulation-demodulation process in the case of $\theta\approx\pi/2$:

$$N=\frac{1}{\hbar\omega_{\mu\mu'}}\int_0^{t_d}P_d(t)dt$$

$$=\frac{1}{4}\frac{\beta}{\beta+1}N_a|\Delta_i|^2e^{-2\gamma T}\frac{k}{\gamma}(1-e^{-2\gamma t_d})\mathrm{sech}^2 A(T). \quad (22)$$

III. FREQUENCY STABILITY

In this section we examine the main physical effects limiting the frequency stability of the POP clock.

A. Thermal and shot noises

The fundamental limit to the frequency stability of a passive pulsed standard is the white frequency noise, coming from the thermal and shot noises, that affects the detected signal; in terms of Allan standard deviation $\sigma_y(\tau)$, the well-known relation holds:

$$\sigma_y(\tau)=\frac{1}{\pi Q_a\mathcal{R}}\sqrt{\frac{T_C}{\tau}}, \quad (23)$$

where $\mathcal{R}$ is the signal-to-noise ratio; it may be expressed in terms of the thermal signal-to-noise ratio $\mathcal{R}_{th}$ and of the shot component $\mathcal{R}_{sh}$ as follows:

$$\mathcal{R}^{-2}=\mathcal{R}_{th}^{-2}+\mathcal{R}_{sh}^{-2}. \quad (24)$$

The thermal noise background added to the microwave detected signal is expressed as

$$\mathcal{R}_{th}=\sqrt{\frac{\hbar\omega_{\mu\mu'}N}{Fk_BT_0}}, \quad (25)$$

where F is the noise figure of the low-noise amplifier (LNA) at the input of the heterodyne detector, k_B the Boltzmann constant, and T_0 the operating cavity temperature. We express here the thermal limit in a different way with respect to that of Ref. [7], introducing the number of the detected microwave photons N for an easier comparison to the shot noise limit.

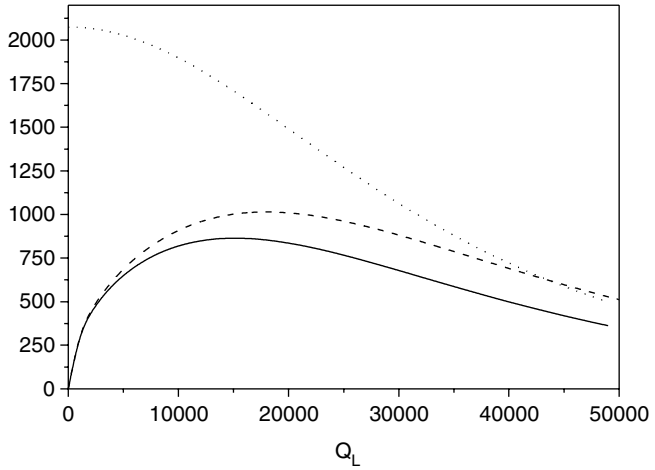

FIG. 6. Signal-to-noise ratios; dash line: $\mathcal{R}_{th}$; dot line: $\mathcal{R}_{sh}$; continuous line: total $\mathcal{R}$; $\Gamma_p=10\,000\ \mathrm{s}^{-1}$, $T_0=336$ K, $t_p=4$ ms, and $t_d=2$ ms.

The detection of N microwave photons implies otherwise a counting process typically obeying to Poissonian statistics (see, for example, [15]). In our pulsed system the following physical considerations have to be taken into account. The atom-cavity interaction introduces a significant correlation among the N detected photons, so that the number of uncorrelated detected events is lower than N. In fact, taking into account the cavity coherence time $\tau_c=Q_L/\omega_{\mu\mu'}$ and the energy-time uncertainty principle $\hbar\omega_{\mu\mu'}\tau_p\approx\hbar$, τ_p^{-1} being the "photon bandwidth," it turns out that the cavity packs the energy in several bunches of about $\tau_c/\tau_p=Q_L$ photons each. This effect is very similar to the Purcell effect [16] related to the change of the number of radiator modes per unit volume and unit frequency induced by the cavity in the weak coupling limit. The uncorreleted counts are then reduced by [17] $Q_L\lambda_0^3/(4\pi^2V_c)$, V_c being the cavity volume and λ_0 the wavelength of the microwave transition. In our case $V_c\approx\lambda_0^3$, so that we may write

$$\mathcal{R}_{sh}=2\pi\sqrt{\frac{N}{Q_L}}. \quad (26)$$

Using Eqs. (22) and (24)–(26), the behavior of $\mathcal{R}$ vs Q_L may be found, as reported in Fig. 6 for a typical set of operating parameters (Secs. IV and V). The signal-to-noise ratio is typically due to thermal noise for $Q_L\ll 4\pi^2Fk_BT_0/\hbar\omega_{\mu\mu'}$ and to shot noise in the opposite case and may be optimized with a proper choice of the cavity Q factor.

B. Cavity pulling

We discuss first the dependence of the POP frequency on the temperature due to the cavity-pulling effect. From Eqs. (19) and taking into account Eqs. (3), (17), and (18) we have

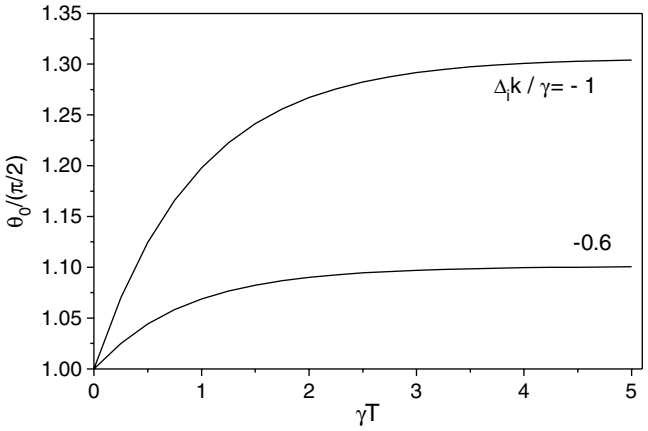

FIG. 7. Zero cavity-pulling value of θ_0 vs Ramsey time.

$$\frac{\Delta\omega_{cp}}{\omega_{\mu\mu'}} = -\frac{4}{\pi}\frac{Q_L}{Q_a}\frac{\Delta\omega_c}{\omega_{\mu\mu'}}\ln\{\cosh A(T) - \mathrm{sgn}(\Delta_i)\cos\theta\sinh A(T)\}. \tag{27}$$

From the above expression we may easily find that a value θ_0 for the microwave pulses exists that cancels the cavity pulling:

$$\theta_0 = \cos^{-1}\left\{\mathrm{sgn}(\Delta_i)\tanh\frac{A(T)}{2}\right\}. \tag{28}$$

A plot of θ_0 vs the normalized Ramsey time γT is reported in Fig. 7 for two values of $\Delta_i k/\gamma$; an increase of the cavity feedback and/or of γT increases the departure of the zero cavity-pulling value θ_0 from $\pi/2$.

Coming back to Eq. (27), it is reasonable, in an experiment, to set the value $\theta \approx \theta_0$ so that the logaritmic term is reduced to 0.005; with $Q_L/Q_a = 10^{-4}$ the cavity detuning must be stable at the level of ±100 Hz in order to achieve a clock frequency stability of 1×10^{-14}. We will see in the next section the implications of this constraint on the design of the thermal control of the microwave cavity.

C. Temperature effects

The hyperfine frequency is also shifted by the buffer gas-atom collisions [5] by

$$\Delta\nu_{\mu\mu'} = P(\beta_b + \delta_b\Delta T + \gamma_b\Delta T^2), \tag{29}$$

where P is the buffer gas pressure, β_b is the pressure coefficient, δ_b and γ_b are the linear and quadratic temperature coefficients, and ΔT is the deviation with respect to the temperature at which the coefficients are measured. The use of a mixture of buffer gas with opposite linear coefficients allows one to achieve a temperature sensitivity of about $\pm1\times10^{-11}$/K.

Spin exchange collisions between alkali-metal atoms are a source of relaxation that causes a broadening of the resonance line proportional to the atomic density; this effect is taken into account in the coherence relaxation rate γ_2. Moreover, they produce a phase shift in the wave function of the atom resulting in a frequency shift $\Delta\omega_{se}$ of the resonance line given by [5]

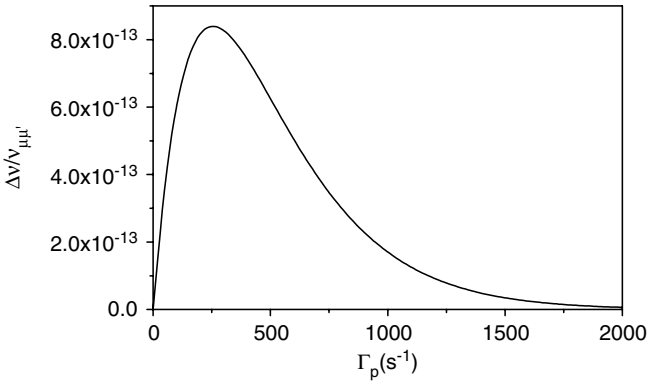

FIG. 8. Output frequency vs the pumping rate due to AM-FM conversion; t_p=4 ms, $T=t_d$=3.3 ms, $\gamma_1=\gamma_2=300\ \mathrm{s}^{-1}$, and $\epsilon=-0.06$.

$$\Delta\omega_{se} = -\frac{1}{4}n\bar{v}\lambda_{se}\langle\Delta\rangle_T, \tag{30}$$

where $\bar{v}$ is the average velocity of two colliding atoms, λ_{se} is the frequency shift cross section, and $\langle\Delta\rangle_T$ is the average value of the population inversion during the Ramsey time T. For ^{87}Rb the temperature dependence of $\Delta\omega_{se}$ has been evaluated in Ref. [18] for operating conditions similar to those of our experiment and turns out to be about $+1\times10^{-11}$/K.

D. Laser noise

The transfer of laser amplitude and frequency fluctuations to the microwave signal is fully rejected in the limiting case of very high laser intensity ($\Gamma_p\to\infty$), as it may be easily seen from Eq. (11) or from the inequality (12) for an optically thick medium. For a limited laser intensity, a residual transfer still remains as we are going to evaluate. The residual light shift effect has been evaluated by considering the transfer of laser amplitude and frequency fluctuations to the frequency of the hyperfine transition, the so called AM-FM (amplitude-to-frequency) and FM-FM (frequency-to-frequency) conversions. We proved in Ref. [7] that this effect is reduced to zero when $\theta=\pi/2$ for all the atoms. Due to possible spatial inhomogeneities it is more practical to consider an effective operating condition where $\theta=\pi/2+\epsilon$ with $\epsilon\ll\pi/2$.

The shift of the central Ramsey fringe may be found in steady state conditions through a recursive numerical solution of Eq. (10); in particular, the following analytical solution holds when $k/\gamma\leqslant1$:

$$\frac{\Delta\omega}{\omega_{\mu\mu'}} = \frac{2\epsilon}{\pi Q_a}\frac{\left(\frac{2\Delta_0}{\Gamma^*} - \frac{\Gamma^*}{2\omega_{\mu\mu'}}\right)\Gamma_p t_p}{1+\cosh(\gamma_2 T_C + \Gamma_p t_p)}. \tag{31}$$

Figure 8 shows the dependence of the relative frequency shift vs the pumping rate Γ_p as predicted by Eq. (31) when $\Delta_0=0$ (off-resonant light-shift) and with the indicated set of parameters.

The AM-FM conversion factor $\partial(\Delta\omega/\omega_{\mu\mu'})/\partial(\Delta\Gamma_p/\Gamma_p)$ may be easily deduced and turns out of the order of $5\times10^{-15}/\%$ for $\Gamma_p t_p=5$ and $\epsilon=0.1$. The linear frequency shift of the output signal vs the laser frequency detuning $\Delta_0/2\pi$ may be evaluated as well from Eq. (31) and for the set of parameters already considered leads to a FM-FM conversion factor $\partial(\Delta\omega/\omega_{\mu\mu'})/\partial(\Delta_0/2\pi)\approx10^{-14}/\mathrm{MHz}$.

As far as it concerns the transfer of the laser AM and FM fluctuations to the output signal amplitude (AM-AM and FM-AM conversions), they may be considered as an additive-type noise. Their effect on the frequency stability may be estimated with a procedure similar to that reported above. It is possible to show that the spectral densities of the laser amplitude and frequency noises are transferred to the output signal divided by Q_a^2 and sampled around the cycling frequency. Moreover, the AM laser noise is further reduced by the saturation factor $(\gamma_1/\Gamma_p)^2$ and the FM laser noise by the factor $(\epsilon\Gamma_p t_p e^{-\Gamma_p t_p})^2$. In the next section, we will show that in usual operating conditions they are negligible.

E. Microwave noise

The fluctuations of the applied microwave field affect the frequency stability mainly via the Dick effect [21] and the cavity-pulling effect. The former is related to the phase fluctuations (FM) of the synthesized microwave signal and the latter to its amplitude instability (AM). In the case of a pulsed frequency standard the Dick limit is given by

$$\sigma_y^2(\tau)=\left\{\sum_{k=1}^{\infty}\mathrm{sinc}^2\left(k\pi\frac{T}{T_C}\right)S_y^{LO}(kf_C)\right\}\tau^{-1}, \tag{32}$$

where $\mathrm{sinc}(x)=\sin x/x$ and $S_y^{LO}(f)$ is the power spectral density of the microwave fractional frequency fluctuations.

The conversion factor for the AM microwave noise may be obtained from Eq. (27) and for $\theta\approx\pi/2$ it turns out:

$$\left.\frac{\partial\left(\frac{\Delta\omega}{\omega_{\mu\mu'}}\right)}{\partial\theta/\theta}\right|_{\theta=\pi/2}=-2\frac{Q_L}{Q_a}\frac{\Delta\omega_C}{\omega_{\mu\mu'}}\,\mathrm{sgn}(\Delta_i)\tanh A(T). \tag{33}$$

Assuming $Q_L/Q_a\approx10^{-4}$ and a cavity detuning $\Delta\omega_c/2\pi\leqslant100$ Hz, Eq. (33) yields a conversion factor of the order of $2\times10^{-14}/\%$ when $|\Delta_i|\frac{k}{\gamma}\approx1$ and $\gamma T\approx1.2$.

F. Position-shift effect

The position-shift effect, first discussed by English *et al.* [8], is due to inhomogeneity in the physics package that makes the resonant frequencies of the rubidium atoms dependent on the location within the cell. The inhomogeneity is mainly due to the nonuniformity of the rf field of the TE_{011} cavity mode, to the laser absorption along the z axis, and to the laser Gaussian mode. The optical pumping and the microwave interrogation are not fully uniform over the cell so that the experimentally observed resonant frequency is a weighted average of the frequencies of the single atoms in the cell. This weighted average changes with the laser intensity and mimics the light-shift behavior (pseudo-light shift). To fully describe this effect it is necessary to solve Eqs. (1) without the approximations $\omega_R=$const and $H_{az}=$const. The numerical solutions indicate that it is possible to limit significantly the position shift effect reducing the cell dimensions approximately at half of those of the cavity and increasing the laser intensity to ensure a full pumping of the atoms (see Sec. V).

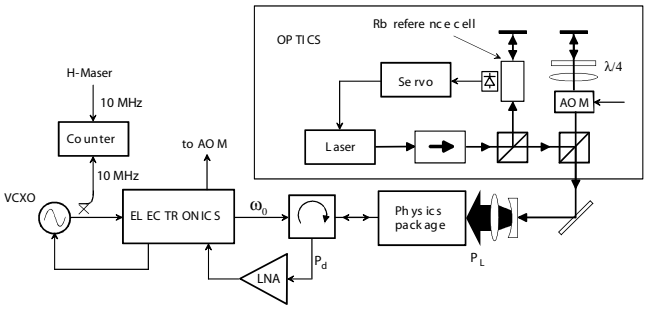

FIG. 9. Experimental setup. LNA: low-noise amplifier.

IV. EXPERIMENTAL SETUP

The experimental setup reported in Fig. 9 shows the main blocks of the system: physics package, optics, and electronics. The physics package is the core of the POP frequency standard and is shown in Fig. 10. The quartz cell has a diameter $2R=30$ mm and a length $L=18$ mm; it contains the ^{87}Rb vapor and a mixture of buffer gases, Ar and N_2 in the pressure ratio 1.6 to 1 to minimize the linear temperature coefficient δ_b [see Eq. (29)] at the operating temperature T_0. The total buffer gas pressure is $P=25$ Torr. The buffer gas induced hyperfine frequency shift is $\Delta\nu_{\mu\mu'}\approx4.28$ kHz ($\beta_b=172$ Hz/Torr) and the quadratic coefficient is $\gamma_b=-7.3\times10^{-4}$ Hz/K^2 Torr [19]. The optical shift due to the buffer gas is $\Delta\nu_{\mu' m}=-170$ MHz and the excited state decay rate is $\Gamma^*=3\times10^9$ s^{-1}.

The cavity is made of aluminum and the resonating mode at $\nu_{\mu\mu'}$ is the TE_{011}; the loaded quality factor is $Q_L=10\,000$, the coupling factor is $\beta=1/2$, and the filling factor is $\eta'=0.3$. The resonance frequency $\nu_c=\omega_c/2\pi$ has a temperature sensitivity $\Delta\nu_c/\Delta T=-160$ kHz/K; the atmospheric pressure

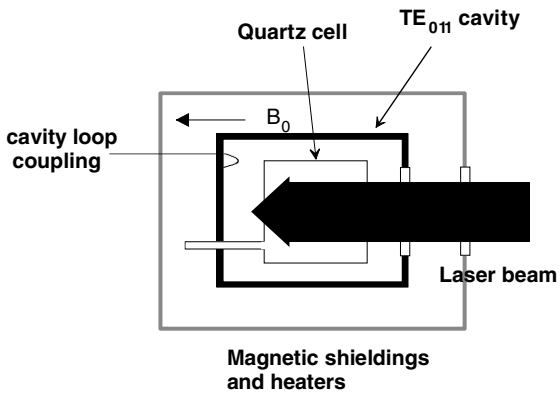

FIG. 10. Physics package.

and humidity sensitivities have been estimated, respectively, $\Delta\nu_c/\Delta P=-10$ Hz/Pa and $\Delta\nu_c=-4$ kHz for a change of 1% of the relative humidity. The operating temperature $T_0 \approx 336$ K has been chosen in order to reach the highest atom number N_a without increasing in a significant way the decay rates γ_1 and γ_2 for spin-exchange and the cell optical length ζ. At this temperature we have $n=4\times10^{11}/\text{cm}^3$, $\alpha=7.7\times10^{11}$ m^{-1} s^{-1}, $\zeta=4.6$, $\gamma_1\approx\gamma_2=300$ s^{-1}, $k/\gamma_2=1.1$, and $N_a=5.6\times10^{11}$ (when $n_e=0.25n$).

Three magnetic shields, two closed-cell polyurethane thermal insulators, and two temperature controlled heaters surround the microwave cavity. The measured temperature standard deviation σ_T of the cavity is $\sigma_T\leqslant100$ μK for measuring times $\tau\leqslant20\,000$ s. Finally, the applied quantization field is $B_0=2$ μT.

In the optic section, a semiconductor laser with an external cavity provides a tunable radiation at 795 nm and a power up to 100 mW; the laser linewidth is $\Delta\nu_L<1$ MHz. Its frequency is locked through a first-order control loop to the $|^2S_{1/2};F=2\rangle-|^2P_{1/2};F=1\rangle$ transition via the Lamb-dip observed in an external cell containing ^{87}Rb. The main part of the laser beam is sent to the physics package through an acousto-optic modulator (AOM) operating in the double-pass configuration. The AOM acts as an optical switch to perform the pulsed pumping of the atoms and shifts the laser frequency towards the red to match the absorption frequency in the clock cell whose frequency is shifted by the buffer gas. The laser beam at the input of the cell is expanded to a diameter $2\rho_w=20$ mm and its intensity is $I_L\approx10$ mW/cm^2; the corresponding pumping rate is $\Gamma_p=120\,000$ s^{-1}. From the computations reported in Fig. 4 we get for the effective atomic density $n_e\approx n/4$ when $t_p\geqslant1$ ms. The laser leakage during the Ramsey and detection times (off state) has been measured to be −60 dB with respect to the on state; the long term amplitude stability is of the order of 1%.

In the electronic section a synthesizer provides the two microwave pulses for the Ramsey interaction, a heterodyne detector is enabled during the detection window and a servo provides the error signal to lock the quartz oscillator at 10 MHz to the Rb clock transition. All the electronic systems operate in a gated mode following the timing sequence of Fig. 2; more details will be provided in Ref. [20]. We recall here only the following data: (i) microwave pulse area stability $\Delta\theta/\theta\leqslant1\times10^{-3}$ for $\tau\leqslant20\,000$ s, (ii) heterodyne detector thermal noise $Fk_BT_0=5\times10^{-21}$ J, and (iii) heterodyne bandwidth BW 200 kHz. Finally, the quartz oscillator phase spectral density $S_y^{LO}(f)$, including also the synthesizer noise, is

$$S_y^{LO}(f)=5\times10^{-27}f+5\times10^{-30}f^{-2}\ \text{Hz}^{-1}. \tag{34}$$

Inserting Eq. (34) in Eq. (32) the expected Dick limit to the frequency stability for a square-wave frequency modulation is $\sigma_y(\tau)\approx7\times10^{-13}\tau^{-1/2}$ for a cycle time $T_C\approx8$ ms and $T=4.6$ ms.

V. EXPERIMENTAL RESULTS

The free-induction decay signal shown in Fig. 11 is observed at the cavity output through a spectrum analyzer operating in the video mode. The decay between the two microwave pulses is due to the combined effect of atom-buffer gas collisions and of the radiation damping; its shape, proportional to $M^2(t)$, is well-described by Eq. (16). In the detection interval the decay is mainly due to the collisions ($e^{-2\gamma t}$) as already assumed in Sec. II. The record has been obtained with $\theta\approx\pi/2$ and $\Omega_\mu/2\pi=10$ Hz; the area defined by the decay signal during t_d is proportional to the detected photon number at that detuning [see Eq. (22)]. The fast decay of the signal after the detection interval is due to the coherence destruction caused by the laser pumping pulse; it guarantees that inequality (12) is widely satisfied in our case, where $t_p=1$ ms and $\Gamma_p\approx12\times10^4$ s^{-1}. The power level of the signal at the end of the first Ramsey pulse is 40 pW and is a factor of 3 lower than the value predicted by Eq. (20); this

FIG. 11. Observed free induction decay. Horizontal: 10 ms/div, vertical: 5 dB/div; resolution bandwidth (RB)=30 kHz, video bandwidth (VB)=30 kHz; timing sequence: $t_p=1$ ms, $t_1=400$ μs, $T=4.6$ ms, and $t_d=2$ ms.

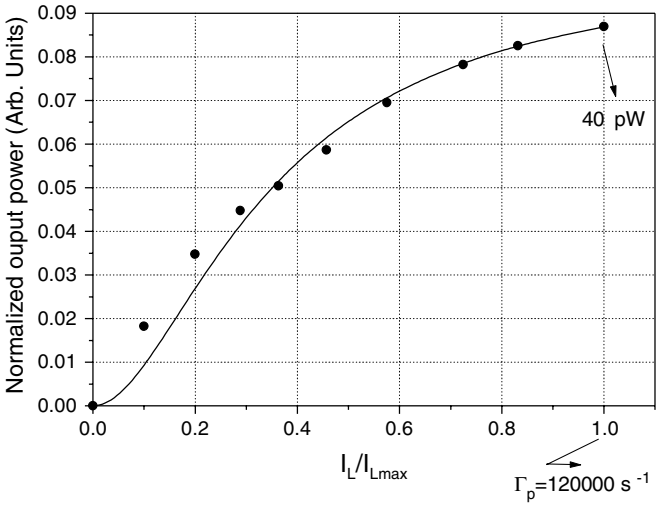

FIG. 12. Measured output power vs laser intensity $t_p=1$ ms, $t_1=400$ μs, $T=4.6$ ms, $t_d=2$ ms, and $I_{L\,\max}=10$ mW/cm^2 ($\Gamma_p=120\,000$ s^{-1}). Circle: experimental values; and continuous line: theory.

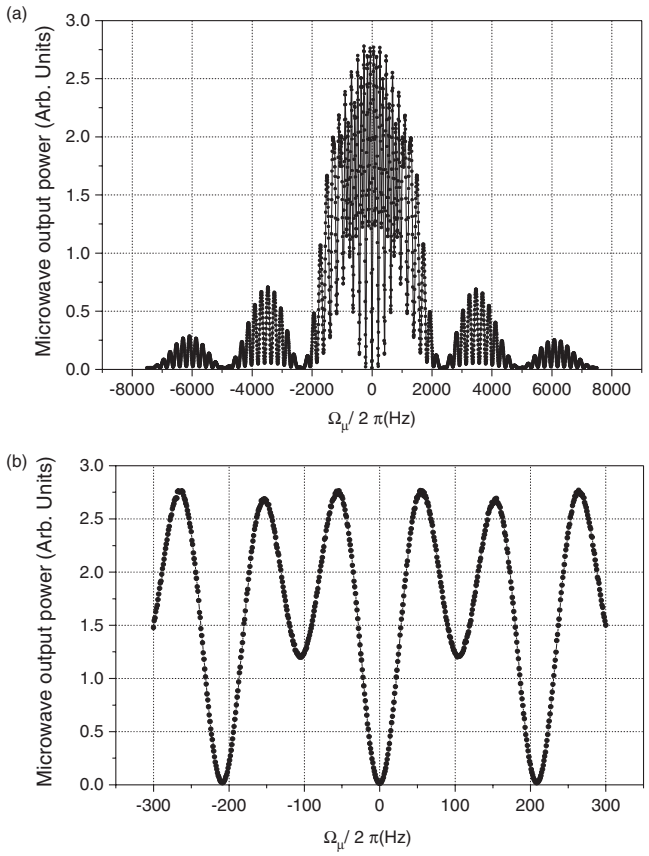

FIG. 13. Interference Ramsey fringes: (a) full pattern; and (b) central fringes. $t_p=1$ ms, $t_1=400$ μs, $T=4.6$ ms, $t_d=2$ ms, $\Gamma_p=120\,000$ s^{-1}, and $\theta=\pi/2$.

discrepancy is due to the nonuniformity of H_{az} and Γ_p within the cell as discussed in Secs. II and III F. Moreover, it is important to remind one that in the experimental conditions the atom experiences a position-dependent microwave field so that the pulse area θ has to be intended in the "average" sense.

The normalized values of the measured power after the first $\pi/2$ pulse are reported in Fig. 12 vs the pumping rate Γ_p for $t_p=1$ ms. They are proportional to $(n_e\Delta_i)^2$ and are in good agreement with the theoretical curve obtained from Eq. (13) and the numerical results of Fig. 4, as shown in the same Fig. 12.

The full pattern of the Ramsey fringes is shown in Fig. 13(a), where the detected number of microwave photons is reported (arbitrary units) vs the frequency detuning $\Omega_\mu/2\pi$. The characteristic shape, reversed and doubled [7], of the central Ramsey fringe is shown in Fig. 13(b); the central one has a FWHM of $\Delta\nu_{1/2}=54$ Hz ($Q_a=1.2\times10^8$) only defined by the free-decay time $T=4.6$ ms and is centered at $\nu_{\mu\mu'}=6\,834\,686\,958$ Hz ($\Omega_\mu=0$).

In Fig. 14 we report the measured value of the noise variance vs the mean value of the detected signal; the points are obtained considering the stochastic process $x(t)$ defined by 740 acquisitions of the detection decay signal and reporting in the figure the variance σ_x^2 vs the average value $\bar{x}$ for each time t in the interval $0\leqslant t\leqslant t_d$. The linear dependence of σ_x^2 vs $\bar{x}$ is due to the squaring operation that provides a signal

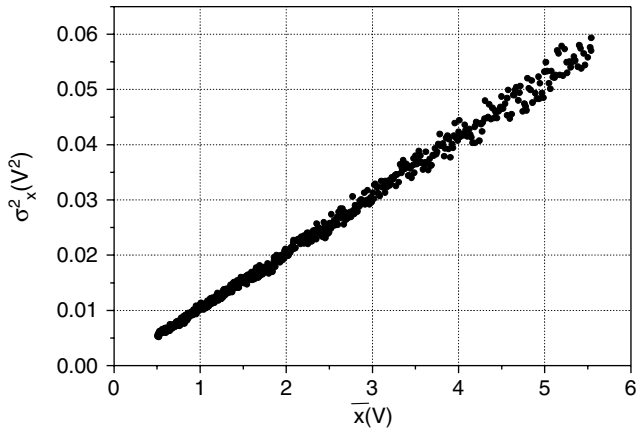

FIG. 14. Variance vs average value of the detected signal; $\Omega_\mu/2\pi=60$ Hz, $t_p=4$ ms, $t_1=600$ μs, $T=4$ ms, $t_d=4$ ms, $I_L=0.6$ mW/cm^2, and $\theta=\theta_0$.

proportional to the microwave power at the detector output.

In Fig. 15 we report the measured $\mathcal{R}$ vs the detection time t_d, obtained in the same operating conditions of Fig. 14. Taking into account the effective operation of the quartz servo implemented in our electronic system, the experimental $\mathcal{R}$ at t_d has been evaluated as

$$\mathcal{R}=\frac{1}{\sigma_A}\int_0^{t_d}P_d(t)dt, \tag{35}$$

where σ_A is the standard deviation of the area defined by the integral in the right-hand side of Eq. (35). In this case, detection times higher than $t_d\approx2$ ms are no longer useful to improve the frequency stability $\sigma_y(\tau)$ [Eq. (23)] because the increase of $\mathcal{R}$ is marginal with respect to the increase of the dead-time and hence of T_C. The experimental result gives a $\mathcal{R}$ lower than the predicted value of Fig. 6 by a factor of 4. This discrepancy is due also in this case to the nonuniformity of H_{az} and Γ_p within the cell.

The relative frequency of the quartz oscillator, locked to the hyperfine transition, vs the laser intensity is reported in Fig. 16 and has been obtained with $\epsilon=\theta-\pi/2=0.05$ and $15<\Gamma_p t_p<120$. The comparison with the calculated AM-FM conversion given by Eq. (31) makes clear that the experimental data are not due to the residual light-shift effect, which is expected two orders of magnitude lower, but may be well due to the position-shift effect discussed in Sec. III E. Anyway, for $\Gamma_p\approx30\,000$ s^{-1} we observe $(\Delta\nu/\nu)/(\Delta I_L/I_L)<10^{-14}/\%$ which is at least three orders of magnitude lower than that observed in the rf-optical double resonance approach [5]. The position shift introduces also a coupling between the laser and the microwave powers observed in the experiments: the microwave power, for example, realizing $\theta=\pi/2$ (minimum detected signal at $\Omega_\mu=0$) slightly depends on the laser intensity. As far as the FM-FM conversion is concerned, we have measured in the same operating conditions of Fig. 16 $(\Delta\nu/\nu)/\Delta\nu_L<10^{-13}$/MHz in agreement with the theoretical prediction of Eq. (31).

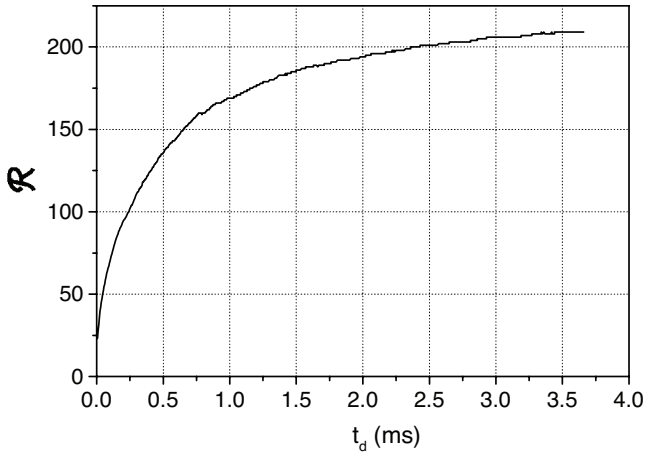

FIG. 15. Measured signal-to-noise ratio vs the detection time.

In Fig. 17 we report the dependence of the POP maser frequency vs θ (microwave field) for three cavity frequency detunings. These data are fully explained through the cavity-pulling effect; in particular the existence of a zero-cavity-pulling value at $\theta=\theta_0=1.05(\pi/2)$ is easily observed, as predicted by Eq. (28). Moreover, the slopes of the curves agree with Eq. (33). In practice, the fine-tuning of the cavity may be done looking for the minimum slope of the ν-θ curve.

In Fig. 18 we report the measured frequency stability of the POP maser at low laser intensity: $I_L \approx 0.8$ mW/cm^2 ($\Gamma_p \approx 10\,000$ s^{-1}). The timing sequence is $t_p=4$ ms, $t_1=600$ μs, $T=4$ ms, and $t_d=2$ ms; the microwave pulse area is $\theta=1.07(\pi/2)$ (zero cavity-pulling).

In these operating conditions we have $\Delta_i \approx -1$, $n_e \approx 0.15n$, $k/\gamma=0.65$, and $N_a=3.3\times10^{11}$; from the relations reported in Secs. II and III A we get $\sigma_y(\tau)=1.1\times10^{-12}\tau^{-1/2}$ that is in satisfactory agreement with the experimental result $\sigma_y(\tau)=1.8\times10^{-12}\tau^{-1/2}$, taking into account that the theoretical prediction is for an optically thin cell and $H_{az}=$const. The medium term stability is limited by a drift of $|\Delta\nu/\nu|=3\times10^{-13}$/day which was found to be highly correlated to the atmospheric pressure with a sensitivity of 10^{-15}/Pa. The drift-removed data show a white frequency trend up to 10^5 s

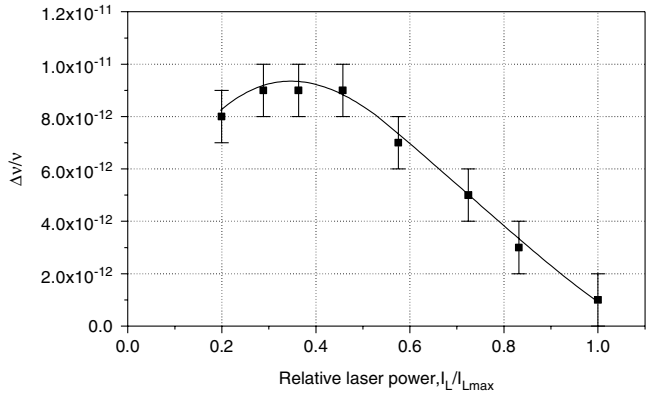

FIG. 16. Frequency vs laser intensity $t_p=1$ ms, $t_1=400$ μs, $T=4.6$ ms, $t_d=2$ ms, and $I_{L\,\max}=10$ mW/cm^2 ($\Gamma_p=120\,000$ s^{-1}).

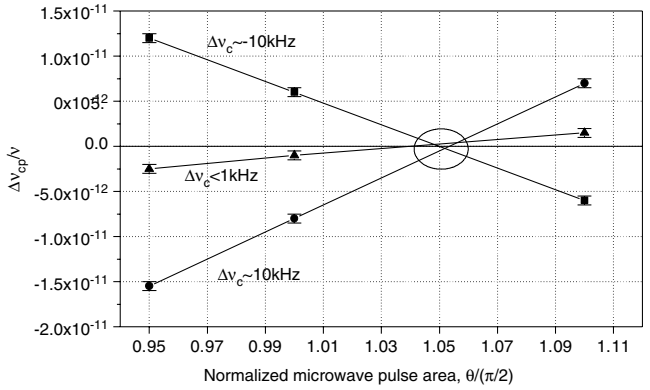

FIG. 17. Cavity-pulling shift vs θ. In the area inside the ellipse the zero-cavity pulling point is highlighted. $t_p=1$ ms, $t_1=400$ μs, $T=4.6$ ms, $t_d=2$ ms, and $\Gamma_p=120\,000$ s^{-1}.

without encountering flicker or random-walk noise contributions. We also provide the Theo1 deviation [22] that is a statistical tool unbiased for the white frequency noise, useful to predict the frequency stability over long times. The reference oscillator for the measurement reported in Fig. 18 is an active autotuned H-maser whose stability is always better than $\sigma_y(\tau)=3\times10^{-13}\tau^{-1/2}$ for $3<\tau<10^5$ s as it turns out when compared with the IEN-CsF1 atomic fountain [23].

The frequency stability reached at high laser intensity ($I_L=10$ mW/cm^2) is shown in Fig. 19 where the timing sequence is now $t_p=1$ ms, $t_1=400$ μs, $T=4.6$ ms, and $t_d=2$ ms. It represents the best stability achieved with our system after a drift removal of $|\Delta\nu/\nu|=6\times10^{-14}$/day, that is $\sigma_y(\tau)=1.2\times10^{-12}\tau^{-1/2}$. Taking into account the Dick limit evaluated in Sec. IV, the thermal noise limited stability is $\sigma_y(\tau)=1\times10^{-12}\tau^{-1/2}$. The experimental results of Figs. 18 and 19 have been obtained with a quartz servoloop having a time constant of 100 ms. Furthermore, the best stability values are obtained with a square-wave frequency modulation depth of ±10 Hz, much less than the FWHM linewidth ($\Delta\nu_{1/2}=50-60$ Hz). This may be explained taking into ac-

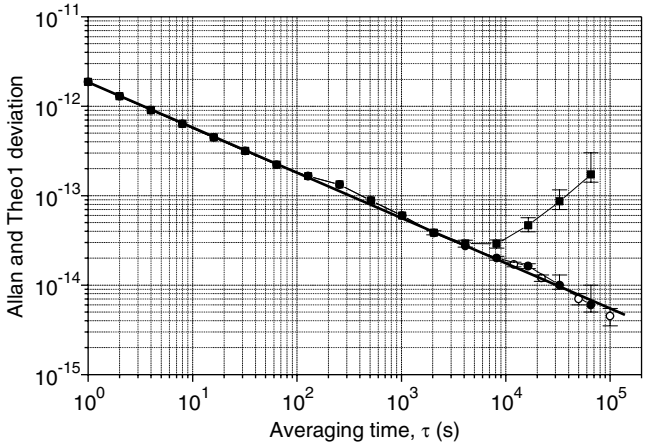

FIG. 18. Frequency stability at low laser intensity. Black square: overlapping Allan deviation (raw data); black circle: overlapping Allan deviation (drift removed data); and open circle: Theo1 standard deviation.

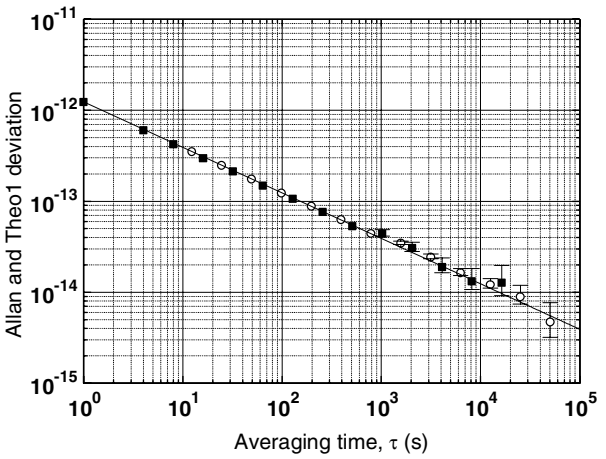

FIG. 19. Frequency stability at high laser intensity. Black square: overlapping Allan deviation; and open circle: Theo1 deviation.

count the dependence of the noise variance vs the signal level reported in Fig. 14.

VI. CONCLUSIONS

In this paper we have first recalled the basic theory that describes the operation of the POP maser with some extensions to that reported in Ref. [7]. In particular, the effects related to the nonuniformity of the microwave and laser fields inside the cell have been examined and, among them, the position-shift. The role of the radiation damping has been also cleared up and made explicit in the equations. We have then analyzed the different noise sources that limit the frequency stability in the short and medium terms, showing the contribution of the themal noise and of the microwave photons shot noise enhanced by the atom-cavity coupling.

The experimental results have been found in good agreement with the theoretical predictions: (i) negligible light-shift; (ii) significant reduction of the cavity-pulling effect with a proper choice of the microwave pulse energy ($\propto\theta$); and (iii) white frequency noise up to the 10^{-15} region after drift removal. The frequency stability obtained with our laboratory prototype is among the best achieved with the state of the art of the secondary frequency standard based on rubidium or cesium vapor cells and is equal to that reported for passive H-masers [24] developed for space applications.

Further improvements aiming to reduce the phase noise of the microwave synthesizer, to optimize the cavity coupling and Q-factor, as well as the atomic active volume and the buffer gas pressure, may lead to a short-term stability $\sigma_y(\tau) \approx 5\times10^{-13}\tau^{-1/2}$ and to a frequency drift of the order of 1×10^{-14}/day.

The results reported here make the POP maser very attractive in all those fields in which the short and medium term stability is a major concern, but also where a simple, compact, and reliable implementation is required.

ACKNOWLEDGMENTS

The authors are grateful to J. Vanier for valuable discussions and suggestions and would like to thank D. Calonico, E. K. Bertacco, and P. P. Capra for useful technical support.

[1] G. Mileti, Jinquan Deng, F. L. Walls, D. A. Jennings, and R. E. Drullinger, IEEE J. Quantum Electron. **34**, 233 (1998); Y. Ohuchi *et al.*, in *Proceedings of the 2000 IEEE International Frequency Control Symposium*, edited by the IEEE Ultrasonics, Ferroelectrics, and Frequency Control Society (IEEE, Kansas City, 2000), pp. 651–655; T. J. Lynch and W. J. Riley, in *Proceedings of the 15th Precise Time and Time Interval (PTTI) Applications and Planning Meeting*, edited by J. A. Murray (Naval Research Laboratory, Washington, 1984), pp. 269–279; C. Affolderbach, F. Droz, and G. Mileti, IEEE Trans. Instrum. Meas. **55**, 429 (2006); J. C. Camparo and R. P. Frueholz, J. Appl. Phys. **59**, 3313 (1986).

[2] T. Zanon, S. Guerandel, E. de Clercq, D. Holleville, N. Dimarcq, and A. Clairon, Phys. Rev. Lett. **94**, 193002 (2005); M. Merimaa, T. Lindvall, E. Tittonen, and E. Ikonen, J. Opt. Soc. Am. B **20**, 273 (2003); R. Wynands, J. Kitching, H. G. Robinson, and L. Hollberg, *ibid.* **18**, 1545 (2001); M. Zhu and L. S. Cutler, in *Proceedings of 32th Precise Time and Time Interval Meeting, Reston, VA*, 2000, edited by L. Breakiron (USNO, Washington, 2000), pp. 311–322; M. Zhu, in *Proceedings of the Joint Meeting 17th European Frequency and Time Forum and 2003 IEEE International Frequency Control Symposium*, Tampa, FL, 2003, edited by J. Vig (IEEE, New York, 2003), pp. 16–21.

[3] A. Godone, F. Levi, S. Micalizio, and C. Calosso, Phys. Rev. A **70**, 012508 (2004).

[4] A. Godone, S. Micalizio, C. E. Calosso, and F. Levi, IEEE Trans. Ultrason. Ferroelectr. Freq. Control **53**, 525 (2006).

[5] J. Vanier and C. Audoin, *The Quantum Physics of Atomic Frequency Standards* (Adam-Hilger, Bristol, England, 1989).

[6] C. O. Alley, in *Quantum Electronics*, edited by C. H. Townes (Columbia University Press, New York, 1960).

[7] A. Godone, S. Micalizio, and F. Levi, Phys. Rev. A **70**, 023409 (2004).

[8] T. C. English, E. Jechart, and T. M. Kwon, in *Proceedings 10th Precise Time and Time Interval Forum*, Washington, 1978, edited by L. J. Rueger (NASA, Maryland, 1979), pp. 147–165.

[9] F. Levi, C. Novero, A. Godone, and G. Brida, IEEE Trans. Instrum. Meas. **46**, 126 (1997).

[10] Y. H. Zou and N. Bloembergen, Phys. Rev. A **33**, 1730 (1986).

[11] A. Godone, F. Levi, and S. Micalizio, *Coherent Population Trapping Maser* (C.L.U.T. Editrice, Torino, Italy, 2002).

[12] F. Levi, A. Godone, and J. Vanier, IEEE Trans. Ultrason. Ferroelectr. Freq. Control **47**, 466 (2000).

[13] S. Bloom, J. Appl. Phys. **27**, 785 (1956).

[14] A. Godone, F. Levi, S. Micalizio, and J. Vanier, Phys. Rev. A **62**, 053402 (2000).

[15] M. O. Scully and M. S. Zubairy, *Quantum Optics* (Cambridge

University Press, Cambridge, England, 1999).
[16] E. M. Purcell, Phys. Rev. **69**, 681 (1946).
[17] H. Walther, B. T. H. Varcoe, B. G. Englert, and T. Becker, Rep. Prog. Phys. **69**, 1325 (2006).
[18] S. Micalizio, A. Godone, F. Levi, and J. Vanier, Phys. Rev. A **73**, 033414 (2006).
[19] J. Vanier, R. Kunski, N. Cyr, J. Y. Savard, and M. Tetu, J. Appl. Phys. **53**, 5387 (1982).
[20] C. Calosso *et al.* (unpublished).
[21] G. Kramer, in *Proceedings of the Conference on Precision Electromagnetic Measurements* (The Institution of Electrical Engineers (London, 1974), p. 157–159; A. Joyet, G. Mileti, G. Dudle, and P. Thomann, IEEE Trans. Instrum. Meas. **50**, 150 (2001).
[22] D. A. Howe and T. K. Peppler, in *Proceedings of the Joint Meeting 17th European Frequency and Time Forum and 2003 IEEE International Frequency Control Symposium*, edited by the IEEE Ultrasonics, Ferroelectrics, and Frequency Control Society (IEEE, Tampa, FL, 2003), pp. 233–238.
[23] F. Levi, L. Lorini, C. Calonico, and A. Godone, IEEE Trans. Ultrason. Ferroelectr. Freq. Control **51**, 1216 (2004).
[24] P. Rochat *et al.*, in *Proceedings of the 2005 Joint IEEE International Frequency Control Symposium and Precise Time and Time Interval (PTTI) Systems and Applications Meeting, Vancouver, Canada* (IEEE, New York, 2005), pp. 26–32.